ACS Photonics

pubs.acs.org/journal/apchd5

Perspective

Tale of Two Resonances: Waveguide–Plasmon Coupling and High *Q*-Factor Engineering on the Nanoscale

Yang Fu,[#] Ye Ming Qing,[#] Zhiyong Li, Anatoly V. Zayats, and Dangyuan Lei*

Cite This: *ACS Photonics* 2023, 10, 2–12

Read Online

ACCESS | Metrics & More | Article Recommendations

ABSTRACT: Localized surface plasmon (LSP) excitations provide an efficient strategy for advancing nanophotonic designs and applications where strong field enhancement and confinement are often required on the nanoscale. They represent an important plasmonic paradigm for achieving strong light–matter interactions in both linear and nonlinear regimes, enabling the development of high-performance chemical and biological sensing approaches and nonlinear optics with low light intensities. However, the LSP resonance line width, limited by both radiative and resistive losses of metallic nanostructures, is significantly larger than the line width of the waveguided modes supported by low-loss dielectric microcavities with a significantly lower field confinement. Hybrid microcavity–plasmonic systems are, therefore, often used to reduce the resonant line width which improves the detection spectral resolution while maintaining strong confinement. Employing the remarkable quality factors of whispering gallery mode (WGM) microresonators, the hybrid LSP-WGM systems demonstrate sensing capabilities down to the single-molecule level. In this Perspective, we review the recent advances in the hybridization of LSPs and WGMs, focusing on the fundamental understanding of the underlying coupling mechanisms and corresponding mode hybridization regimes. We further discuss opportunities for applying heterogeneous plasmonic–photonic integration to tailor the nanoscale light–matter interactions and realize novel waveguide–plasmon coupling based nontrivial responses and highlight their prospective applications in quantum optics, chiral spin-optics, nonlinear nanophotonics, and sensing.

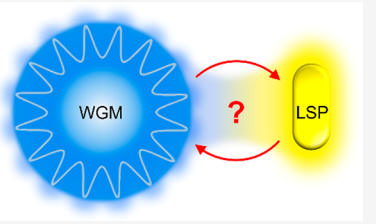

KEYWORDS: *localized surface plasmon, whispering gallery mode, quality factor, mode hybridization, strong coupling*

Free electrons in nanostructured metals can be driven by an electromagnetic field to undergo collective in-phase oscillation, resulting in the excitation of localized surface plasmons (LSPs), which strongly enhance the electromagnetic near-field intensity and far-field scattering. The LSPs can be well described by the analytical Mie theory or numerical full-wave electromagnetic simulations.[1] The LSP-induced near-field enhancement and confinement within a deep subwavelength mode volume can boost a variety of linear and nonlinear optical processes and related applications, including surface-enhanced Raman scattering, photoluminescence, photothermal therapy, high-contrast label-free bioimaging, data storage, harmonic generation, and many others.[2−9] However, LSPs undergo dephasing and decay on the femtosecond time scales and hence exhibit a broad spectral line width, that is, a low quality-factor (*Q*-factor),[10,11] which is unfavorable and even detrimental for many nanophotonic applications. Typically, the LSP spectral line width of individual gold nanoparticles is on the order of several tens of nanometers in the visible spectral range.[12,13] Significant efforts have been made to narrow the LSP resonance line width by suppressing the radiative damping in metallic nanostructures. For example, delicate design of nanoparticle arrays allows coupling of the LSPs of the constituent particles with the diffraction-induced surface lattice resonance of the array, thereby shrinking the LSP line width down to ∼5 nm.[14] On the other hand, coupling LSPs to a low-loss dielectric microcavity makes it possible to achieve hybrid photonic-plasmonic modes with resonance line widths down to the subnanometer level.[15] In these hybrid systems, the spectral line width modification depends on the intrinsic *Q*-factor of the cavity resonance mode to which the LSP resonance is coupled and on their coupling strength.

In the previous studies, optical (micro)cavities, such as Fabry-Pérot cavities,[16] Bragg microcavities,[17] whispering gallery mode[18] (WGM) resonators, and photonic crystals[19] have been exploited as effective platforms for coupling with plasmonic nanostructures and reducing the LSP line width. Typically, these photonic microcavities have high *Q*-factors[20] and may serve as building blocks for microscale lasers,[21] sensors,[22] filters,[23,24] and so on. Among them, photonic WGMs, an analogue of acoustic WGMs,[25,26] have drawn considerable attention due to their remarkable *Q*-factors of over 10^8.[27,28] The evanescent fields residing at the surface of a WGM microresonator are highly sensitive to the surrounding

Received: August 16, 2022
Revised: November 19, 2022
Accepted: November 21, 2022
Published: December 5, 2022

dielectric environment and provide a sensing platform with an extraordinary spectral resolution.

The LSP-WGM coupling can be used not only to improve the LSP resonance line width, but also to modify the overall optical response of the hybrid system, such as a resonant frequency, a scattering spectral profile, and so on. On the one hand, when a hybrid LSP-WGM system is excited via one of its waveguide eigenmodes, the LSP resonance, invoked through near-field coupling, in turn modulates the WGM spectral profile and hence may improve the WGM sensitivity, through the plasmon-induced near-field enhancement, to tiny variations in the local dielectric environment, such as the index of refraction of the cavity material itself or the adsorption of nanoparticles and biochemical molecules onto the microcavity surface.[29] It has been reported that sensitivity down to the single-molecule level can be achieved in such LSP-WGM hybrid systems benefiting from the plasmonic enhancement.[30] Line width broadening and mode splitting of bare WGMs can also be manipulated through plasmonic coupling.[31,32] On the other hand, under the far-field excitation by free-space illumination, the LSP mode of the hybrid system is first activated as a base resonance and then modulated by the excitation of WGMs. Importantly, the resonance spectrum of the hybrid LSP-WGM system varies nonmonotonically as the diameter of the WGM microresonator decreases, resulting in a dominant spectral peak with a line width as narrow as 2 nm.[33−35]

In this Perspective, we first introduce the fundamentals of LSP and WGM resonances and hybrid plasmonic−photonic systems. We then discuss characteristic optical responses of the hybrid resonances and elaborate corresponding coupling mechanisms by using the coupled-oscillator model and a Fourier transform method. We conclude with the outlook of further developments of hybrid waveguide−plasmon systems and highlight potential opportunities for their applications in achieving complex optical responses required in modern nanophotonic applications.

LSP AND WGM RESONANCES

LSP. Metallic nanoparticles (MNPs) with typical sizes larger or comparable to the metal skin depth support LSPs and enable the near-field enhancement and extreme confinement of an incident optical field. Various nanostructured noble metals, such as gold, silver, platinum, etc., in the shapes of spheres, rods, cubes, triangles, and stars have been fabricated to achieve a required plasmonic response at the wavelengths ranging from the UV to the near-infrared.[36−45] In addition, metallic core−shell constructs and nanoparticle assemblies have proven to sustain more versatile LSP modes and endow more degrees of freedom in tailoring the light−matter interactions at the nanoscale.[46−48] Typically, the LSP-induced near-field intensity enhancement for a single MNP, that is, $|E|^2/|E_0|^2$, where E_0 and E are the electric field amplitudes of the incoming light and the local field at the surface of the MNP, respectively, can vary from ten-folds to thousand-folds, depending on its size and shape.[12,49−52] Larger enhancement factors can be obtained by delicately assembling MNPs into clusters or arrays.[53,54] Figure 1a−d illustrates the electric near-field intensity enhancement profiles of several classical LSP-resonant metal nanostructures, exhibiting hot spots with extremely localized near-fields under the excitation of their dipolar plasmon resonance modes.

The collective electron oscillations, corresponding to the excitation of LSPs, and the induced near-field enhancement

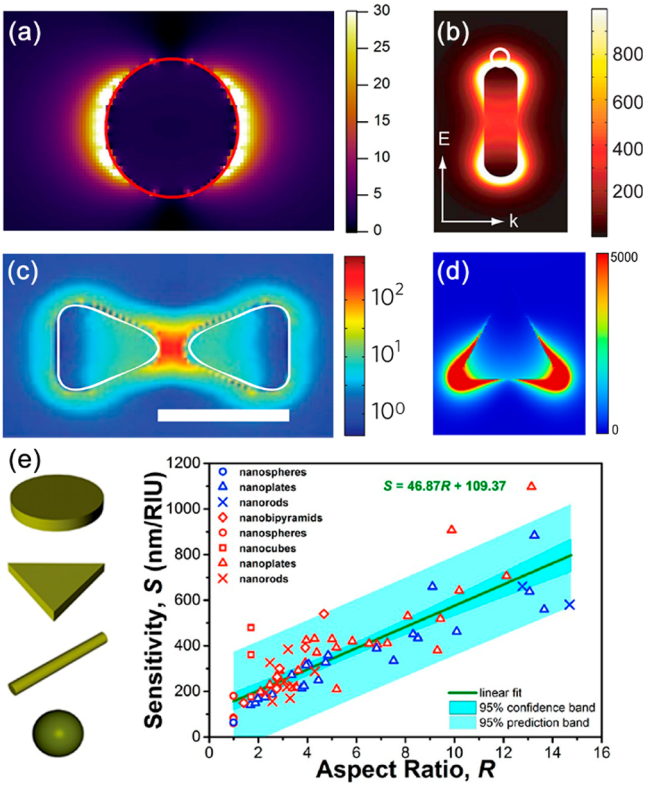

Figure 1. Near-field intensity enhancement profiles for (a) a gold nanosphere,[50] (b) a gold nanorod,[51] (c) a gold nanoprism dimer,[55] and (d) a silver nanotriangle.[52] (e) Refractive index sensitivity of the LSPs supported by gold nanoparticles with varying aspect ratio.[56] (a) Reprinted with permission from ref 50. Copyright 2012 The Optical Society. (b) Reprinted with permission from ref 51. Copyright 2011 AIP Publishing. (c) Reprinted with permission from ref 55. Copyright 2009 Nature Publishing Group. (d) Reprinted with permission from ref 52. Copyright 2016 Nature Publishing Group. (e) Reprinted with permission from ref 56. Copyright 2016 American Chemical Society.

and confinement near a MNP determines its resonance frequency sensitivity to the local dielectric environment, namely, the refractive index of the medium located within and nearby the near-field hot spot region. Moreover, tailoring the key geometric parameters of MNPs, for example, the aspect ratio of gold nanorods, provides easy-to-implement means for engineering the sensitivity of LSP-based sensors,[56] which can be optimized to reach values up to 1000 nm/RIU (Figure 1e).

WGM. The optical counterpart of acoustic WGMs was first observed as a high-Q optical resonance mode in a dielectric microsphere.[57] Upon being coupled to the microsphere, the light path is bent through the total internal reflection at the curved dielectric-air boundary, so that the coupled light recirculates in the structure for a long time.[58] When the optical path of the light accumulated over one propagation cycle satisfies the condition of constructive interference, that is, equal to an integer multiple of the light wavelength, a standing electromagnetic wave can be established along the perimeter of the microsphere. Spatially, the dielectric microsphere can trap light typically at a micrometer scale; temporally, its high Q-factor WGM allows light to propagate in the cavity for millions of cycles. Such spatial and temporal confinement of light in the microsphere is accompanied by an intensive evanescent-field tail outside the curved boundary, which empowers an elegant platform for investigating many cavity-enhanced physical

https://doi.org/10.1021/acsphotonics.2c01271
ACS Photonics 2023, 10, 2−12

processes, such as cavity quantum electrodynamics and nonlinear optics, and also for constructing a variety of photonic devices, such as microlasers and biosensors.[20,33,59]

The optical WGMs can be supported in a variety of dielectric microresonators. The fundamental mechanism for forming WGMs can be intuitively understood in the structures with the spherical or cylindrical symmetry using the Mie scattering theory.[60] For microstructures of asymmetric geometries or higher-order symmetries, analytical treatment is no longer feasible, and one has to resort to full-wave numerical simulations to simulate their field distribution profiles. *Q*-factor, which is frequently used to evaluate the merit of WGM microresonators, is determined mainly by the radiation loss and materials absorption:[28,61]

$$Q = \omega\tau = \frac{\omega}{\omega_{\mathrm{FWHM}}} = \frac{\lambda}{\lambda_{\mathrm{FWHM}}} \tag{1}$$

where τ is the cavity ring-down time, ω (or λ) is the angular frequency (or wavelength) of the resonant mode, and fwhm is the full-width at half-maximum of the resonance. Other parameters, such as the mode volume, determining the spatial confinement of optical energy, and the free space range (FSR), characterizing the spectral distance between two adjacent resonance peaks, are also used for evaluating a WGM resonator.

HYBRID LSP-WGM SYSTEMS

Integrating a plasmonic MNP at the exterior vicinity of a WGM microresonator forms a hybrid LSP-WGM system, which is able to harness both resonances for manipulating the light−matter interaction on the nanoscale. Here, we will introduce the hybrid LSP-WGM systems under two typical excitation scenarios: near-field excitation and free-space illumination. In the former case, the MNP in a hybrid system is regarded as an external perturbation and provides sensitivity enhancement of the WGMs through the near-field hotspot.[62] In the latter case, the WGM modulates the characteristic spectral response of the coupled LSP mode and boosts its *Q*-factor. The coupled-oscillator model and a Fourier transform method will be discussed in the following in order to analyze different coupling regimes between these two resonances.

Near-Field Excitation. In this excitation scenario, the WGMs are excited by coupling the evanescent wave of a tapered fiber/waveguide/prism to an adjacent WGM resonator (Figure 2). When a MNP is placed in the vicinity of the microresonator, WGM resonance shift, line width broadening, and mode splitting can be observed. The wavelength shift can be estimated by applying the first-order perturbation theory as[58]

$$\frac{\Delta\lambda}{\lambda} \approx \frac{\alpha |E(\mathbf{r_A})|^2}{2\int \epsilon(\mathbf{r})|E(\mathbf{r})|^2 \, \mathrm{d}V} \tag{2}$$

where α and $\mathbf{r}_A$ are the polarizability and position of the MNP, respectively. The WGM line width broadening associated with both absorption and scattering losses introduced by the coupled MNP can be calculated as[58]

$$\frac{\delta\lambda_{\mathrm{abs}}}{\lambda} \approx \frac{\mathrm{Im}[\alpha]|E(\mathbf{r_A})|^2}{2\int \epsilon(\mathbf{r})|E(\mathbf{r})|^2 \, \mathrm{d}V} \tag{3}$$

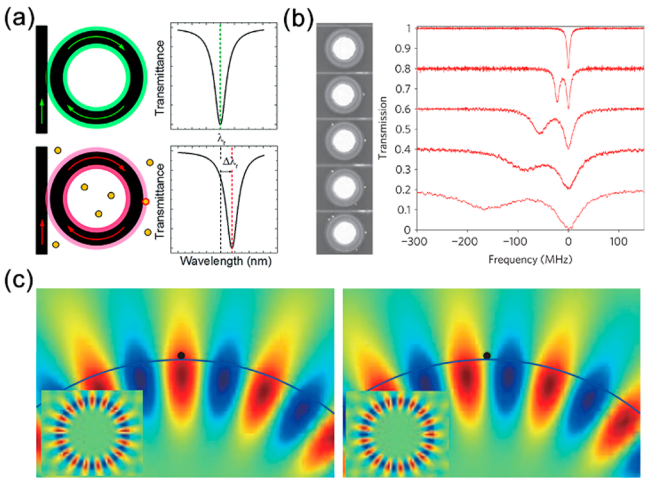

Figure 2. (a) Schematic illustration of waveguide-based near-field excitation of the WGM in a microring resonator and the WGM resonance shift induced by the adsorption of MNPs.[63] (b) The dependence of mode splitting and line width broadening in the transmission spectrum of a WGM on the number of adsorbed KCl nanoparticles, from top to bottom: 0−4.[64] (c) Simulated electric field distributions of (left) symmetric and (right) antisymmetric modes induced by coupling to a nanoparticle indicated by a black dot.[64] (a) Reprinted with permission from ref 63. Copyright 2017 The Royal Society of Chemistry. (b, c) Reprinted with permission from ref 64. Copyright 2009 Nature Publishing Group.

$$\frac{\delta\lambda_{\mathrm{sca}}}{\lambda} \approx \frac{4\pi^3 c n_0^5 \epsilon_0}{3\lambda^4} \frac{|\alpha|^2 |E(\mathbf{r_A})|^2}{\int \epsilon(\mathbf{r})|E(\mathbf{r})|^2 \, \mathrm{d}V} \tag{4}$$

where n_0 is the refractive index of the WGM microresonator, c is the speed of light, and ϵ_0 is the permittivity of vacuum.

Besides inducing extra losses, the presence of a nanoparticle can also lift the degeneracy of two standing wave modes in a microresonator, resulting in mode splitting. When light is coupled into a WGM cavity and travels as a clockwise mode (CW), it can be scattered by an adsorbed nanoparticle back into the cavity as a counterclockwise mode (CCW) with a phase delay compared to the CW mode. Two standing wave patterns are then formed inside the cavity as a result of the interference between the CW and scattered-CW (the same wavelength) and the CW and scattered-CCW (at a longer wavelength). Notably, the mode splitting and line width broadening often coexists in the WGM (Figure 2b). Such self-referenced hybrid system exhibits two distinctive near-field distribution profiles, corresponding to a symmetric and an antisymmetric modes of the system, respectively.[32,64] As shown in Figure 2c, the nanoparticle lies in the near-field antinode of the symmetric mode and at the node of the antisymmetric mode.

The spectral modulation described above is related to the interaction between the evanescent-field tail of the WGM and the nanoparticle in the local environment of the waveguide. It is also worth noting that the WGM resonant wavelength shift and line width change (eqs 2−4) are proportional to the local field intensity, $|\boldsymbol{E}(\mathbf{r_A})|^2$, which can be significantly enhanced at the LSP-induced near-field hot spot. In another words, hybridization with LSPs is capable of improving the sensitivity of a WGM microresonator to its environment. For a bare WGM microresonator (usually with a diameter of tens of micrometers), the WGM resonance shifts were experimentally

https://doi.org/10.1021/acsphotonics.2c01271
ACS Photonics 2023, 10, 2−12

observed up to 650 fm at the operation wavelength of 1311 nm.[65] In the presence of the MNPs, the hybrid system exhibited a resonance shift of 4 pm and a fractional wavelength shift $\Delta\lambda/\lambda$ up to 6×10^{-6},[66] which is over 1 order of magnitude higher.[63,65,67−70]

Such hybrid LSP-WGM systems have emerged as a high-performing label-free sensing platform (Figure 3). Shopova et

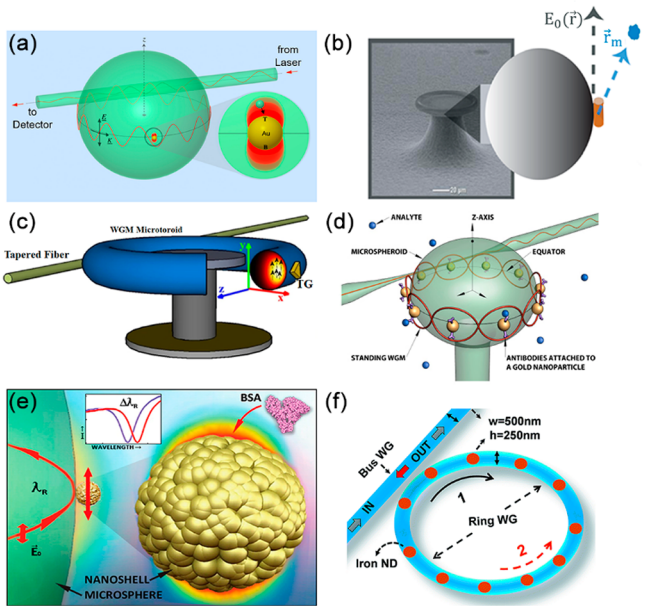

Figure 3. Hybrid LSP-WGM systems under the near-field excitation. (a) Au nanoshell coupled to a microsphere for PS nanoparticle detection.[29] (b) Au nanorod coupled to a microtoroid for BSA detection.[51] (c) Au nanotriangle coupled to a microtoroid for BSA detection.[71] (d) Periodic Au nanoparticles coupled to a microsphere for virus detection.[72] (e) Rough Au nanosphere coupled to a microsphere for BSA detection.[73] (f) Fe nanodisk array coupled to a microring for bulk refractive index sensing.[74] (a) Reprinted with permission from ref 29. Copyright 2011 AIP Publishing. (b) Reprinted with permission from ref 51. Copyright 2011 AIP Publishing. (c) Reprinted with permission from ref 71. Copyright 2015 AIP Publishing. (d) Reprinted with permission from ref 72. Copyright 2012 The Optical Society. (e) Reprinted with permission from ref 73. Copyright 2013 American Chemical Society. (f) Reprinted with permission from ref 74. Copyright 2016 The Royal Society of Chemistry.

al. demonstrated the capturing and detection of individual polystyrene (PS) nanoparticles in aqueous environment with a stationary gold nanoshell, bound to a dielectric microsphere equator (Figure 3a),[29] and observed a resonance shift enhancement by a factor of 4, compared to the WGM without the MNP. By replacing the gold nanoshell with a gold nanorod with aspect ratio of 4 (Figure 3b), Swain et al. performed numerical prediction of a ∼870-fold enhancement in resonance shift for bovine serum albumin (BSA) detection, which is much higher than the measurement noise arising from time-averaged frequency and thermal fluctuations.[51] Nadgaran et al. studied the influence of gold nanotriangles with tunable size (Figure 3c) on the WGM resonance shift and found an enhancement factor over 1000 for BSA detection.[71] In addition to single MNPs, Arnold et al. proposed using a periodic array of gold nanoparticles (epitopes) attached to the equator of WGM (Figure 3d); this allowed for more binding sites for capturing analyte and the self-reference induced mode splitting was observed for detection of viruses.[72] With eight viruses adsorbed on the four epitopes, the mode splitting increased from 3.5 to ∼280 fm, which is larger than the resonance line width of the hybrid system (195 fm) and can be easily detected. Further, Dantham et al. reported an extraordinary enhancement of ∼635 in the wavelength shift for detecting BSA proteins, which was ascribed to the roughness of a gold nanoshell (Figure 3e).[73]

Besides detection of particle-like analytes, the hybrid LSP-WGM systems also exhibit superiority in the bulk refractive index sensing. For bare dielectric WGM resonators, such as microrings and microdisks, a typical sensitivity to refractive index changes of the environment is in the range of 50−200 nm/RIU. In the presence of MNPs, it increases to over 500 nm/RIU.[74−77] Table 1 provides a detailed comparison of the sensing capabilities of typical LSPs, WGMs, and hybrid LSP-WGM systems.

Free-Space Excitation. Plasmonic MNPs can serve as optical nanoantennas to convert light from propagating to evanescent waves. Under free-space illumination, the excitation of LSPs in a MNP can couple the incident light to the WGM of a nearby dielectric microresonator through near-field coupling, which provides a more effective and practical strategy for activation of the hybrid system. In this excitation regime, the lossy LSP resonance performs as a broadband near-field source for the WGM, leading to a WGM-modulated spectral profile of the LSP resonance (Figure 4). By tuning the dimension of the WGM microresonator or the size, shape and material of the MNP, the coupling strength between the two resonances can vary from weak to strong and the Q-factor of the hybrid mode often exhibits a nonmonotonic variation.[34] For example, an isolated Au nanorod with aspect ratio of ∼2.5 shows a broad scattering spectrum centered at ∼650 nm with a spectral line width of ∼52 nm. Upon coupling to a microfiber of 25.4 μm in diameter, the broad LSP scattering spectrum was strongly modulated and features a series of sharp subpeaks, corresponding to the waveguide modes of different orders supported by the microfiber (Figure 4b). With a decrease of the microfiber diameter, the number of supported WGMs reduces and their FSR increases, resulting in fewer WGM-modulated subpeaks in the scattering spectrum (Figure 4c). However, as the microfiber diameter continues decreasing, anomalously strong line-shape narrowing occurs with an ultranarrow line width of ∼2 nm and a larger FSR of ∼43 nm (Figure 4d). This effect has been qualitatively ascribed to the strong coupling between the two resonances. Similar strong coupling emergence and line-shape evolution have also been observed in a system of a Pd nanorod coupled to a silica microfiber.[35]

Based on this effect, Zhou et al. demonstrated a multiple-cavity-based distributed optical humidity sensor through depositing periodic Au nanorods on a polyacrylamide microfiber.[78] The properties of this ultranarrow resonance were also used in the nonlinear optical regime: in a gold nanorod-silica microfiber hybrid system,[33] both the linear scattering and nonlinear second-harmonic emission spectra exhibit ultranarrow peaks, which are promising for nonlinear sensing and extremely efficient nonlinear light generation from ultrasmall volumes.

The evolution of a coupling strength can be intuitively understood considering the lifetimes of WGM and LSPs. The LSP lifetime of a gold nanorod is much shorter than the single-cycle dwelling time of a photon in a microcavity with a

https://doi.org/10.1021/acsphotonics.2c01271
ACS Photonics 2023, 10, 2−12

Table 1. Comparison of *Q*-Factors and Sensing Capabilities of LSPs, WGMs, and Hybrid LSP-WGM Systems

ref	resonator structure	resonant wavelength	*Q*-factor	$\Delta\lambda$ or sensitivity	detection target
Khan et al.[56]	Au nanoprism	1030 nm	4.1	884 nm/RIU	refractive index
Martinsson et al.[86]	Au nanosphere	525 nm	7.5	80 nm/RIU	refractive index
Farooq et al.[87]	Au nanorod	589−1603 nm	9.4−13.2	150−772 nm/RIU	refractive index
	Au dimeric nanorod	589−1160 nm	13−24.4		
Iqbal et al.[88]	microring	1565 nm	4.3E4	163 nm/RIU	refractive index
Vollmer et al.[65]	microsphere	763 nm	6.4E5	10−650 fm	single PS bead (200−500 nm)
		1311 nm	2.6E5		single Inf A virus (90−110 nm)
Lu et al.[68]	microtoroid	680 nm	8E6−1E8	0.5−11 fm	single PS bead (25−100 nm); single Inf A virus
Zhu et al.[64]	microtoroid	670 nm	>1E8	15−600 fm	single KCl bead (90−320 nm)
		1450 nm			single PS bead (70−350 nm)
Lee et al.[89]	wedge disk	1500 nm	8.75E8	NA	NA
Wang et al.[34]	microfiber + Au nanorod	660 nm	330	NA	NA
Nadgaran et al.[71]	microtoroid + Au nanotriangle	1500 nm	3.6E4−1.13E5	10−26 fm	single BSA protein
Santiago-Cordoba et al.[66]	microsphere + Au nanospheres	633 nm	1E5	2−4 pm	BSA proteins
Shopova et al.[29]	microsphere + Au nanoshells	633 nm	5E5	90−210 fm	single PS bead (110 nm)
Baaske et al.[30]	microsphere + Au nanorods	780 nm	5E6	2.5 fm	single 8-mer 1 oligonucleotide chain

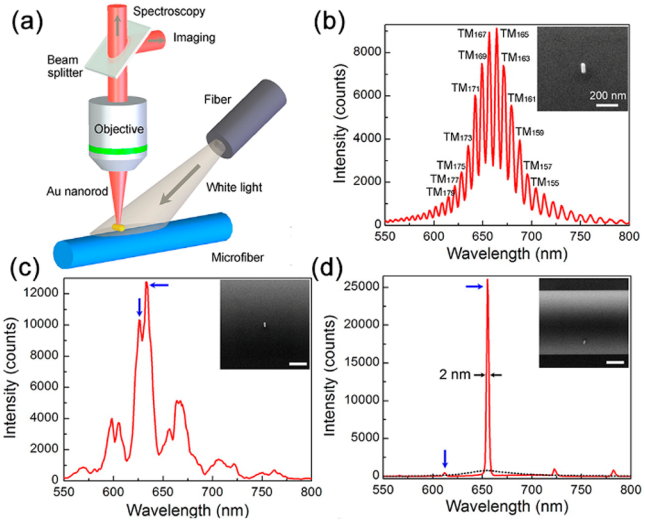

Figure 4. (a) Schematic illustration of free-space excited hybrid LSP-WGM system consisting of a Au nanorod and a silica microfiber. (b−d) Scattering spectra of a Au nanorod coupled silica fibers with diameters of (b) 25.4, (c) 5.6, and (d) 1.46 μm.[34] Insets show corresponding SEM images of Au nanorods on microfibers. (a−c) Adapted with permission from ref 34. Copyright 2015 American Chemical Society.

relatively large diameter. As a result, the photon energy cannot be efficiently exchanged between the two resonances and the weak coupling regime is observed. As the microfiber diameter decreases, the single-cycle dwelling time reduces to below 100 fs and becomes comparable to the LSP lifetime. Thus, the Au nanorod can be re-excited by the cavity photons before the LSPs decay totally. This makes the photon energy store in the hybrid system longer through mode coupling, and the strong-coupling regime is reached.

COUPLED-OSCILLATOR MODEL

To gain an intuitive understanding of the LSP-WGM mode interaction, we apply the coupled-oscillator model (COM) working in the classical framework. COM treats the LSP-WGM coupling as two interacting oscillators coupled together with a spring (Figure 5a). Adopting this model,[79−83] the mode coupling is described by

$$\begin{pmatrix} \omega_l - i\gamma_l & \kappa \\ \kappa & \omega_w - i\gamma_w \end{pmatrix} \begin{pmatrix} \alpha \\ \beta \end{pmatrix} = \omega_{\pm} \begin{pmatrix} \alpha \\ \beta \end{pmatrix} \tag{5}$$

where ω_l and ω_w are the frequencies of uncoupled LSP and WGM resonances, respectively, γ_l and γ_w are their decay rates (i.e., damping rates, resulting in the full width at half-maximum of $2\gamma_l$ and $2\gamma_w$), κ is the coupling strength, α and β are the relative weightings of the LSP and WGM resonances, respectively, in the hybrid mode, with $|\alpha|^2 + |\beta|^2 = 1$. The diagonalization of above matrix yields two eigenvalues

$$\omega_{\pm} = \frac{\omega_l + \omega_w}{2} - \frac{i}{2}(\gamma_l + \gamma_w) \pm \sqrt{\kappa^2 + \frac{1}{4}[\delta - i(\gamma_l - \gamma_w)]^2} \tag{6}$$

with $\delta = \omega_l - \omega_w$ representing the detuning frequency. At zero detuning ($\delta = 0$), eq 6 yields the mode splitting

$$\Omega = \sqrt{4\kappa^2 - (\gamma_l - \gamma_w)^2} \tag{7}$$

which is also called the Rabi frequency. It should be noted that eq 7 has valid solutions only if

$$\kappa > |\gamma_l - \gamma_w|/2 \tag{8}$$

which is the condition of the strong coupling regime. This condition is achieved in Figure 4c,d since the decreased diameter of the microfiber renders the decay rate of a WGM comparable to that of the LSP, that is, $|\gamma_l - \gamma_w|$ approaches zero. In contrast, for $\kappa < |\gamma_l - \gamma_w|/2$, the LSP-WGM interaction is in the weak coupling regime, and the spectral modulation of a broader resonance rather than a mode splitting is observed (Figure 4b).

Figure 5b shows the frequencies of the two modes in different coupling regimes. Far away from the zero detuning, the frequencies of the hybrid modes are approaching the two original modes shown by the dashed line. Near the zero detuning, new hybrid modes at frequencies of $\omega_{\pm}$ appear with characteristic anticrossing behavior (solid lines; the gray

https://doi.org/10.1021/acsphotonics.2c01271
ACS Photonics 2023, 10, 2−12

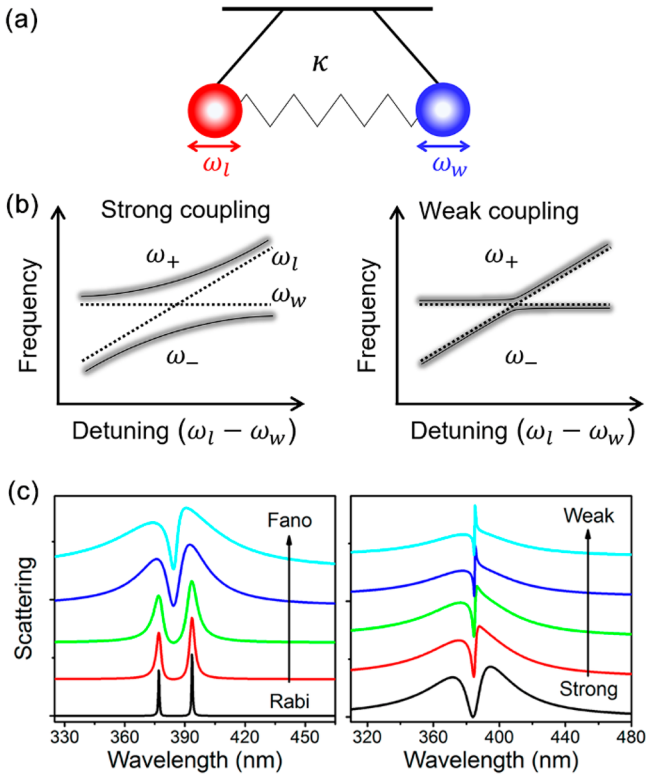

Figure 5. (a) Schematic of two oscillators coupled with a spring. (b) Schematics of the energy levels in strong and weak coupling regimes: the LSP and WGM frequencies (dashed lines) in the absence of coupling, (solid lines) the coupling behavior, and (gray shadow) broadening due to the damping. (c) Schematics of the scattering spectra in various coupling regimes: (left) increasing the value of the damping rate or line width results in a transition from a Rabi splitting regime (strong coupling) to a Fano interference regime (weak coupling), (right) decreasing the value of the coupling constant κ results in a transition from an antiresonance feature in the Lorentzian spectrum to an asymmetric line shape superimposed on the Lorentzian spectrum.[85] (c) Reprinted with permission from ref 85. Copyright 2014 American Chemical Society.

shadow schematically represents damping). In a weak coupling regime, the mode splitting is difficult to identify.

To better observe the splitting of the two hybrid modes, the energy difference should exceed the fwhm of the two modes:

$$\Omega > \gamma_l + \gamma_w \tag{9}$$

Therefore, the coupling strength and damping rates (or line widths) of two resonances are key physical parameters that dictate the nature of mode coupling. In the LSP-WGM systems, the coupling strength depends on how fast and efficient the energy exchange is between the evanescent fields of the WGM resonator and the local field of the nearby MNP. Strong coupling can be achieved with not too lossy WGM and LSP resonances where both conditions (eqs 8 and 9) are satisfied and can easily be spectrally observed in the peak splitting of the scattering spectrum.[34,84]

Figure 5c illustrates a gradual transition from a strong coupling regime, described by Rabi splitting, to a weak coupling regime, described by the Fano interference, for two interacting modes. It should be noted that in the latter case, one of the coupled modes has a broad line width and the other has a narrow one, breaking the condition of eq 8. Fano interference occurs in the far field and results in the spectral profiles with asymmetric line shapes due to phase shift between two modes.[15] A typical observation of such Fano interference is illustrated in Figure 6, where the evolution of constructive

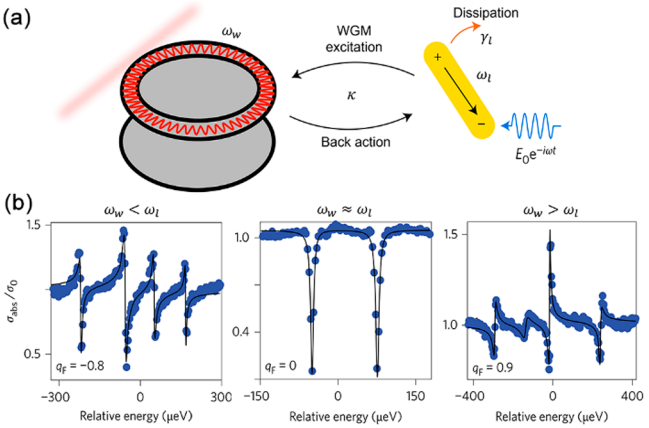

Figure 6. (a) Schematic of coupling between a Au nanorod and a microtoroid. The LSP of the nanorod is excited by the far-field illumination and coupled to a WGM. (b) Experimental spectra fitted with Fano lineshapes when the WGM resonant frequencies (from left to right) are smaller, near to, and larger than the LSP frequency.[15] (a, b) Adapted with permission from ref 15. Copyright 2016 Nature Publishing Group.

and destructive interferences is exemplified by three types of line shapes.[15] Notably, Fano dips, which often occur in the weak coupling regime, should not be mixed up with the Rabi splitting even if they have similar spectral line shapes (e.g., Figures 5c and 6b).

FOURIER-TRANSFORM METHOD

The COM can provide a phenomenological description of the influence of mode coupling on the resonance evolution. The key fitting parameters, such as the coupling strength, eigenfrequency and damping coefficient of each mode, were used to obtain the absorption or scattering spectra of the hybrid systems under either near-field excitation or free-space illumination. However, the exact description of a line shape based on geometric and optical parameters of the hybrid system is less satisfactory reproduced in COM.[15,34,84] We now introduce a semianalytical model, in which the Fourier transformation of time-domain electric field distribution is used in order to evaluate the line width changes in different coupling regimes. In this model, we consider the LSP as a base resonance and the WGM cavity as a time-domain modulation of the LSP. This method was developed for description of the far-field excitation of the hybrid system, for which a strong coupling regime was often demonstrated.

The LSP spectrum can be found from the Fourier transformation of the local electric field of an individual MNP that can be directly obtained from the FDTD simulations:

$$|F\{\boldsymbol{E}^l(t)\}|^2 = \sum_{i=x,y,z} |F\{E_i^l(t)\}|^2 \tag{10}$$

where $E_i(t)$ denotes the electric field components, with $i = x$, y, and z. The WGM time-domain electric field components can be generally expressed as

$$E_i^w(t) = A_i e^{-\gamma_w \cdot t} \tag{11}$$

https://doi.org/10.1021/acsphotonics.2c01271
ACS Photonics 2023, 10, 2−12

where γ_w denotes the decay rate of WGM and A_i is the amplitude of the WGM electric field components. However, in a hybrid nanoparticle−microcavity system, additional phase shift ($\Delta\phi_M$) and cavity elongation (Δd) need to be taken account, induced by the presence of a MNP, so that

$$E_i^w(t) = A_i e^{-\gamma_w \cdot t} e^{-i(\Delta\phi_M + \frac{\omega n \Delta d}{c})} = A_i e^{-\gamma_w \cdot t} e^{-i\Delta\phi} \quad (12)$$

where n is the refractive index of the WGM cavity, ω is the angular frequency at the resonance, c is the speed of light in vacuum, and we combined the additional phase shift and cavity elongation by introducing a total phase change $\Delta\phi$.

The total electric field of the hybrid system is then

$$E_i(t) = E_i^l(t) + \sum_{N=1}^{\infty} E_i^w(NT) \cdot E_i^l(t - NT) \quad (13)$$

where T is the single cycle dwelling time. The scattering spectrum can be obtained through the Fourier transformation of the total electric field $\sum_{i=x,y,z} E_i(t)$.

The electric field components of the hybrid LSP-WGM system with parameters T = 22.8 fs and $\gamma_w = 5 \times 10^{12}$ Hz are shown in Figure 7a, representing the superposition of the

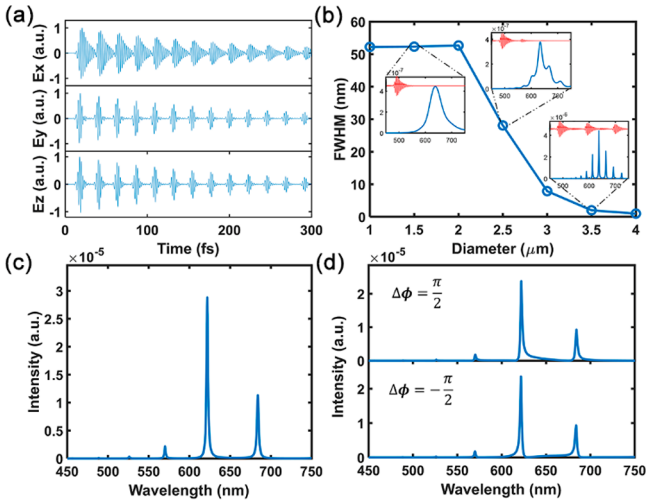

Figure 7. (a) Electric field components of the hybrid LSP-WGM system obtained from eq 13. The original LSP electric field components are extracted from the FDTD simulation. (b) The dependence of the calculated line width on a diameter variation of the WGM cavity. The refractive index is n = 1.45. The quality factors used for calculating the decay rates are extracted from ref 30: T = 15.2 fs and $\gamma_w = 4.5 \times 10^{14}$ Hz for D = 1 μm; T = 22.8 fs and $\gamma_w = 3.2 \times 10^{14}$ Hz for D = 1.5 μm; T = 30.4 fs and $\gamma_w = 1.45 \times 10^{14}$ Hz for D = 2 μm; T = 38 fs and $\gamma_w = 4.8 \times 10^{13}$ Hz for D = 2.5 μm; T = 45.6 fs and $\gamma_w = 1.6 \times 10^{13}$ Hz for D = 3 μm; T = 53.1 fs and $\gamma_w = 4.46 \times 10^{12}$ Hz for D = 3.5 μm; T = 60.7 fs and $\gamma_w = 2.32 \times 10^{12}$ Hz for D = 1.5 μm. Inset: (red line; scale 0−150 fs) time-domain electric field of the hybrid system and (blue line) the Fourier transformed scattering spectra for the indicated diameters. (c, d) Fourier transformed scattering spectra of a WGM cavity with D = 1.5 μm and $\gamma_w = 5 \times 10^{12}$ Hz for the phase modulation (c) $\Delta\phi = 0$ and (d) $\Delta\phi = \pm \pi/2$.

electric fields with cavity decay after every cycle. Based on this approach, the line width evolution of the hybrid LSP-WGM system is illustrated in Figure 7b. Here, the single-cycle dwelling time and the decay rate for a WGM cavity with a diameter of D are calculated from $T = n\pi D/c$ and $\gamma_w \approx \omega/Q$, respectively. All the parameters used in the calculations are extracted from ref 34 for direct comparison. However, the remarkable line width narrowing observed in the experiment in Figure 4d was not obtained for D = 1.5 μm (Figure 7b). Only if a less lossy WGM is considered, a line width of 2 nm can be achieved for a decay rate of $\gamma_w = 5 \times 10^{12}$ Hz (Figure 7c), which is over 1 order of magnitude lower than the experimental data ($\gamma_w = 3.2 \times 10^{14}$ Hz) for the WGM cavity with this diameter. Nevertheless, this model describes the asymmetry feature of the LSP-WGM modes observed in ref 34 (Figure 7d) and reveals how the phase change $\Delta\phi$ affects the symmetry of the spectral line shape without influencing the resonance positions, mimicking the asymmetry factor of the Fano line shape.

OUTLOOK

Benefiting from the ultrahigh Q-factor of WGMs and the LSP-induced local near-field enhancement and confinement, hybrid LSP-WGM systems exhibit versatile optical properties. The spatially overlapping near fields and mode energies exchange dynamically, ensuring strong sensitivity to surroundings with pronounced resonance shift and line width variation. Two excitation strategies, that is, near-field (WGM excitation through a nearby waveguide) and far-field (i.e., free-space excitation of LSP), have been widely studied in terms of their characteristic spectral responses, including mode shift, mode broadening, mode splitting, profile modulation, and anomalous line width narrowing. Two descriptions of the hybrid systems based on a coupled oscillator model, applicable for both excitation regimes, and the Fourier transform method, applicable only to free-space excitation, were discussed. The underlying coupling mechanisms and transition from weak to strong coupling regime in a hybrid system have been well understood through the COM model. The details of the hybrid mode formation can be revealed using the Fourier transform method.

While various sensing and detection applications have been investigated in hybrid LSP-WGM systems, we have identified three main challenges requiring further considerations. First, although the sensitivity of a hybrid system can be improved up to 1 order of magnitude, the limit of detection is restricted by the noise induced by the LSP radiative loss. In the strong coupling regime, the electric field is redistributed due to the coupling effect, which reduces the leakage loss and significantly improves the Q factor. However, a Q-factor of the coupled system is still smaller than that of the isolated microresonators with large diameters (which can be over 10^8).[26,27,89] Advancing materials and structure designs for hybridization with WGMs is imperative in order to achieve lower losses and stronger field confinement, for example, through the use of MNP dimers, trimers, nanocavities, and self-assembled constituents.[90−94]

Second, the field confinement induced by MNPs strongly reduces the active sensing area of a microresonator. Compared to the mode volume of the hybrid system, which is primarily determined by a WGM resonator, the region with the LSP enhanced fields is vastly limited. Though hybrid systems with multiple MNPs along the equator of the WGM resonator have been investigated,[30,72,95] deposition/adsorption of MNPs with high accuracy and density is still very challenging. Top-down fabrication combined with bottom-up growth may help in this respect.[96,97]

Finally, the line width narrowing and side-mode suppression in the strong coupling regime are not well described in the existing models with realistic parameters. Corrections to the

https://doi.org/10.1021/acsphotonics.2c01271
ACS Photonics 2023, 10, 2−12

models introduced here or development of new models with higher conformity and not requiring fitting parameters are required for designing new applications of LSP-WGM hybrid systems.

Nevertheless, by exploiting the ultrasmall mode volume V of LSPs and the extremely high Q-factor of WGMs, the hybrid nanophotonic systems provide an intriguing platform for exploring nontrivial optical responses, including nonlinear optics, chirality and non-Hermitian physics (Figure 8). As the

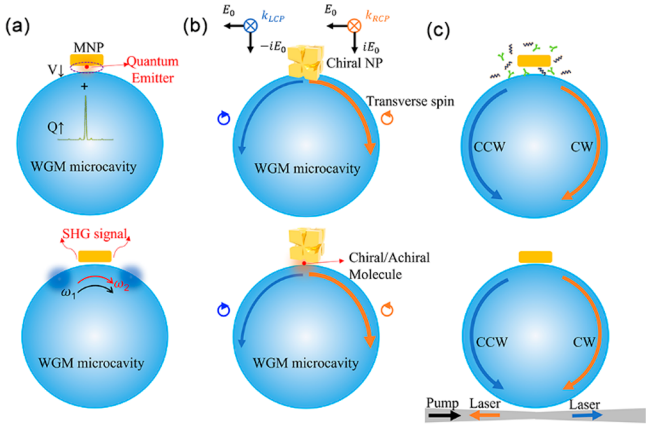

Figure 8. Schematics of LSP-WGM hybrid platforms for (a) ultrastrong coupling regime with high Q-factor and small mode volume V (top), and SHG and high-harmonic enhancement (bottom), (b) spin−orbit interaction induced chiral routing (top) and chiral sensing (bottom), (c) non-Hermitian sensing near exceptional points (top) and non-Hermitian lasing with chiral modes (bottom).

interaction between a quantum emitter and a photonic mode can be enhanced in such hybrid LSP-WGM systems, it may be possible to design a single-photon frequency combs by exploiting the ultrastrong coupling between an array of super-radiant quantum emitters and the hybrid resonant system. Introducing structural asymmetry to the WGM microcavity may induce enhanced second-harmonic generation (SHG). Other nonlinear optical processes can also benefit from strong field enhancement and narrow and controllable resonances of the hybrid systems.[33,98]

Photonic spin−orbit interaction (SOI) harvests a transverse spin at the boundaries of a WGM cavity, providing additional degrees of freedom for manipulating light-matter interactions in a LSP-WGM system. For CW and CCW propagating waves in a WGM cavity, the transverse spin flips the sign due to a spin-momentum locking,[99] which can be coupled to the LSP spin states, determining directional polarized scattering.[100] Alternatively, selective excitation of CW or CCW modes can be achieved using a chiral MNPs under the excitation of circular polarized light.[101,102] By placing quantum dots or molecules in the gap between MNPs and a WGM cavity, chiral quantum routing or chiral sensing can be realized.[103] SOI effects can also be used together with novel chiral materials, such as 2D materials with chiral excitons, for development of valleytronic devices with nonreciprocal functionalities.[104,105]

The difference in the fwhm's of CW and CCW WGMs induced by MNPs provides a foundation for studying non-Hermitian local sensors.[106] Specifically, molecules attached to the surface of a MNP introduce a perturbation (ϵ) of the system and, therefore, a frequency splitting $\Delta f \propto |\epsilon|^{1/N}$ for the Nth order of exceptional points (EPs).[107] By adjusting the system to operate near EPs, the frequency splitting can be sufficiently enhanced. Such a sensor is expected to be more selective and sensitive for detecting small molecules. Although the noise in detection may offset the enhancement in frequency splitting for EP sensors under small perturbations, the sensing precision (i.e., signal-to-noise ratio) can be improved, for example, if operating near the lasing threshold.[108,109] In addition, employing the missing dimension of EPs, non-Hermitian lasing might be achieved in a hybrid system by harnessing directionality of the waveguide mode and the exciting light. This also generates novel chiral modes and opens up a new avenue for developing new light sources for photonic integrated devices.[110,111] The tale of two resonances continues.

AUTHOR INFORMATION

Corresponding Author

Dangyuan Lei − *Department of Materials Science and Engineering, City University of Hong Kong, Kowloon, Hong Kong SAR 999077, China;* orcid.org/0000-0002-8963-0193; Email: dangylei@cityu.edu.hk

Authors

Yang Fu − *Department of Materials Science and Engineering, City University of Hong Kong, Kowloon, Hong Kong SAR 999077, China*

Ye Ming Qing − *Department of Materials Science and Engineering, City University of Hong Kong, Kowloon, Hong Kong SAR 999077, China*

Zhiyong Li − *Department of Electronic Engineering and Materials Science and Technology Research Center, The Chinese University of Hong Kong, Shatin, New Territories, Hong Kong SAR 999077, China;* orcid.org/0000-0002-9062-548X

Anatoly V. Zayats − *Department of Physics and London Centre for Nanotechnology, King's College London, London WC2R 2LS, United Kingdom;* orcid.org/0000-0003-0566-4087

Complete contact information is available at: https://pubs.acs.org/10.1021/acsphotonics.2c01271

Author Contributions

#These authors contributed equally.

Funding

The work is supported by the Research Grants Council of Hong Kong through the ANR/RGC Joint Research Scheme (A-CityU101/20), ERC iCOMM project (789340), and EPSRC CPLAS project (EP/W017075/1).

Notes

The authors declare no competing financial interest.

ACKNOWLEDGMENTS

The authors acknowledge useful discussions with Dr. Hongfei Wang, Mr. Feihong Liu, and Mr. Peigang Chen.

REFERENCES

(1) Li, G.-C.; Zhang, Q.; Maier, S. A.; Lei, D. Plasmonic particle-on-film nanocavities: a versatile platform for plasmon-enhanced spectroscopy and photochemistry. *Nanophotonics* **2018**, *7*, 1865.

(2) Schlücker, S. SERS microscopy: nanoparticle probes and biomedical applications. *ChemPhysChem* **2009**, *10*, 1344.

(3) Mohamed, M. B.; Volkov, V.; Link, S.; El-Sayed, M. A. The lightning' gold nanorods: fluorescence enhancement of over a million compared to the gold metal. *Chem. Phys. Lett.* **2000**, *317*, 517.
(4) Jaque, D.; Maestro, L. M.; Del Rosal, B.; Haro-Gonzalez, P.; Benayas, A.; Plaza, J.; Rodríguez, E. M.; Solé, J. G. Nanoparticles for photothermal therapies. *Nanoscale* **2014**, *6*, 9494.
(5) Hutter, E.; Maysinger, D. Gold nanoparticles and quantum dots for bioimaging. *Microsc. Res. Technol.* **2011**, *74*, 592.
(6) Zhang, S.; Li, G.-C.; Chen, Y.; Zhu, X.; Liu, S.-D.; Lei, D. Y.; Duan, H. Pronounced Fano resonance in single gold split nanodisks with 15 nm split gaps for intensive second harmonic generation. *ACS Nano* **2016**, *10*, 11105.
(7) O'Connor, D.; Zayats, A. V. The third plasmonic revolution. *Nat. Nanotechnol.* **2010**, *5*, 482.
(8) Kauranen, M.; Zayats, A. V. Nonlinear plasmonics. *Nat. Photonics* **2012**, *6*, 737.
(9) Wang, P.; Nasir, M. E.; Krasavin, A. V.; Dickson, W.; Jiang, Y.; Zayats, A. V. Plasmonic metamaterials for nanochemistry and sensing. *Acc. Chem. Res.* **2019**, *52*, 3018.
(10) Sönnichsen, C.; Franzl, T.; Wilk, T.; von Plessen, G.; Feldmann, J.; Wilson, O.; Mulvaney, P. Drastic reduction of plasmon damping in gold nanorods. *Phys. Rev. Lett.* **2002**, *88*, 077402.
(11) Hu, M.; Novo, C.; Funston, A.; Wang, H.; Staleva, H.; Zou, S.; Mulvaney, P.; Xia, Y.; Hartland, G. V. Dark-field microscopy studies of single metal nanoparticles: understanding the factors that influence the linewidth of the localized surface plasmon resonance. *J. Mater. Chem.* **2008**, *18*, 1949.
(12) Amendola, V.; Pilot, R.; Frasconi, M.; Maragò, O. M.; Iatì, M. A. Surface plasmon resonance in gold nanoparticles: a review. *J. Phys.: Condens. Matter* **2017**, *29*, 203002.
(13) Maier, S. A.*Plasmonics: fundamentals and applications*; Springer Science & Business Media, 2007.
(14) Zhou, W.; Odom, T. W. Tunable subradiant lattice plasmons by out-of-plane dipolar interactions. *Nat. Nanotechnol.* **2011**, *6*, 423.
(15) Heylman, K. D.; Thakkar, N.; Horak, E. H.; Quillin, S. C.; Cherqui, C.; Knapper, K. A.; Masiello, D. J.; Goldsmith, R. H. Optical microresonators as single-particle absorption spectrometers. *Nat. Photonics* **2016**, *10*, 788.
(16) Schmidt, M. A.; Lei, D. Y.; Wondraczek, L.; Nazabal, V.; Maier, S. A. Hybrid nanoparticle−microcavity-based plasmonic nanosensors with improved detection resolution and extended remote-sensing ability. *Nat. Commun.* **2012**, *3*, 1.
(17) Khadir, S.; Chakaroun, M.; Belkhir, A.; Fischer, A.; Lamrous, O.; Boudrioua, A. Localized surface plasmon enhanced emission of organic light emitting diode coupled to DBR-cathode microcavity by using silver nanoclusters. *Opt. Express* **2015**, *23*, 23647.
(18) McCall, S.; Levi, A.; Slusher, R.; Pearton, S.; Logan, R. Whispering-gallery mode microdisk lasers. *Appl. Phys. Lett.* **1992**, *60*, 289.
(19) Paul, D.; Biswas, R. Highly sensitive LSPR based photonic crystal fiber sensor with embodiment of nanospheres in different material domain. *Optics & Laser Technology* **2018**, *101*, 379.
(20) Vahala, K. J. Optical microcavities. *Nature* **2003**, *424*, 839.
(21) Samuel, I. D.; Namdas, E. B.; Turnbull, G. A. How to recognize lasing. *Nat. Photonics* **2009**, *3*, 546.
(22) Hanumegowda, N. M.; Stica, C. J.; Patel, B. C.; White, I.; Fan, X. Refractometric sensors based on microsphere resonators. *Appl. Phys. Lett.* **2005**, *87*, 201107.
(23) Matsko, A. B.; Ilchenko, V. S. Optical resonators with whispering-gallery modes-part I: basics. *IEEE J. Sel. Top. Quantum Electron.* **2006**, *12*, 3.
(24) Ilchenko, V. S.; Matsko, A. B. Optical resonators with whispering-gallery modes-part II: applications. *IEEE J. Sel. Top. Quantum Electron.* **2006**, *12*, 15.
(25) Rayleigh, L. CXII. The problem of the whispering gallery. *London, Edinburgh, and Dublin Philosophical Magazine and Journal of Science* **1910**, *20*, 1001.
(26) Rayleigh, L. IX. Further applications of Bessel's functions of high order to the Whispering Gallery and allied problems. *London, Edinburgh, and Dublin Philosophical Magazine and Journal of Science* **1914**, *27*, 100.
(27) Armani, D.; Kippenberg, T.; Spillane, S.; Vahala, K. Ultra-high-Q toroid microcavity on a chip. *Nature* **2003**, *421*, 925.
(28) Gorodetsky, M. L.; Savchenkov, A. A.; Ilchenko, V. S. Ultimate Q of optical microsphere resonators. *Opt. Lett.* **1996**, *21*, 453.
(29) Shopova, S.; Rajmangal, R.; Holler, S.; Arnold, S. Plasmonic enhancement of a whispering-gallery-mode biosensor for single nanoparticle detection. *Appl. Phys. Lett.* **2011**, *98*, 243104.
(30) Baaske, M. D.; Foreman, M. R.; Vollmer, F. Single-molecule nucleic acid interactions monitored on a label-free microcavity biosensor platform. *Nat. Nanotechnol.* **2014**, *9*, 933.
(31) Hu, Y.; Shao, L.; Arnold, S.; Liu, Y.-C.; Ma, C.-Y.; Xiao, Y.-F. Mode broadening induced by nanoparticles in an optical whispering-gallery microcavity. *Phys. Rev. A* **2014**, *90*, 043847.
(32) Subramanian, S.; Vincent, S.; Vollmer, F. Effective linewidth shifts in single-molecule detection using optical whispering gallery modes. *Appl. Phys. Lett.* **2020**, *117*, 151106.
(33) Ai, Q.; Gui, L.; Paone, D.; Metzger, B.; Mayer, M.; Weber, K.; Fery, A.; Giessen, H. Ultranarrow second-harmonic resonances in hybrid plasmon-fiber cavities. *Nano Lett.* **2018**, *18*, 5576.
(34) Wang, P.; Wang, Y.; Yang, Z.; Guo, X.; Lin, X.; Yu, X.-C.; Xiao, Y.-F.; Fang, W.; Zhang, L.; Lu, G.; et al. Single-band 2-nm-line-width plasmon resonance in a strongly coupled Au nanorod. *Nano Lett.* **2015**, *15*, 7581.
(35) Gu, F.; Zhang, L.; Zhu, Y.; Zeng, H. Free-space coupling of nanoantennas and whispering-gallery microcavities with narrowed linewidth and enhanced sensitivity. *Laser Photon. Rev.* **2015**, *9*, 682.
(36) Bonaccorso, F.; Zerbetto, M.; Ferrari, A. C.; Amendola, V. Sorting nanoparticles by centrifugal fields in clean media. *J. Phys. Chem. C* **2013**, *117*, 13217.
(37) Zijlstra, P.; Chon, J. W.; Gu, M. Five-dimensional optical recording mediated by surface plasmons in gold nanorods. *Nature* **2009**, *459*, 410.
(38) Soares, L.; Csáki, A.; Jatschka, J.; Fritzsche, W.; Flores, O.; Franco, R.; Pereira, E. Localized surface plasmon resonance (LSPR) biosensing using gold nanotriangles: detection of DNA hybridization events at room temperature. *Analyst* **2014**, *139*, 4964.
(39) Barbosa, S.; Agrawal, A.; Rodríguez-Lorenzo, L.; Pastoriza-Santos, I.; Alvarez-Puebla, R. A.; Kornowski, A.; Weller, H.; Liz-Marzán, L. M. Tuning size and sensing properties in colloidal gold nanostars. *Langmuir* **2010**, *26*, 14943.
(40) Park, J.; Kang, H.; Kim, Y. H.; Lee, S.-W.; Lee, T. G.; Wi, J.-S. Physically-synthesized gold nanoparticles containing multiple nano-pores for enhanced photothermal conversion and photoacoustic imaging. *Nanoscale* **2016**, *8*, 15514.
(41) Poletti, A.; Fracasso, G.; Conti, G.; Pilot, R.; Amendola, V. Laser generated gold nanocorals with broadband plasmon absorption for photothermal applications. *Nanoscale* **2015**, *7*, 13702.
(42) Wu, H.-L.; Kuo, C.-H.; Huang, M. H. Seed-mediated synthesis of gold nanocrystals with systematic shape evolution from cubic to trisoctahedral and rhombic dodecahedral structures. *Langmuir* **2010**, *26*, 12307.
(43) Wang, H.; Brandl, D. W.; Nordlander, P.; Halas, N. J. Plasmonic nanostructures: artificial molecules. *Acc. Chem. Res.* **2007**, *40*, 53.
(44) Luan, J.; Liu, K.-K.; Tadepalli, S.; Jiang, Q.; Morrissey, J. J.; Kharasch, E. D.; Singamaneni, S. PEGylated artificial antibodies: plasmonic biosensors with improved selectivity. *ACS Appl. Mater. Interfaces* **2016**, *8*, 23509.
(45) Córdova-Castro, R. M.; Casavola, M.; Van Schilfgaarde, M.; Krasavin, A. V.; Green, M. A.; Richards, D.; Zayats, A. V. Anisotropic plasmonic CuS nanocrystals as a natural electronic material with hyperbolic optical dispersion. *ACS Nano* **2019**, *13*, 6550.
(46) Tsai, C.-Y.; Lin, J.-W.; Wu, C.-Y.; Lin, P.-T.; Lu, T.-W.; Lee, P.-T. Plasmonic coupling in gold nanoring dimers: observation of coupled bonding mode. *Nano Lett.* **2012**, *12*, 1648.
(47) Li, G.-C.; Zhang, Y.-L.; Jiang, J.; Luo, Y.; Lei, D. Y. Metal-substrate-mediated plasmon hybridization in a nanoparticle dimer for

photoluminescence line-width shrinking and intensity enhancement. *ACS Nano* **2017**, *11*, 3067.
(48) Wang, P.; Krasavin, A. V.; Viscomi, F. N.; Adawi, A. M.; Bouillard, J. S. G.; Zhang, L.; Roth, D. J.; Tong, L.; Zayats, A. V. Metaparticles: Dressing Nano-Objects with a Hyperbolic Coating. *Laser Photon. Rev.* **2018**, *12*, 1800179.
(49) Sousa-Castillo, A.; Comesaña-Hermo, M.; Rodríguez-González, B.; Pérez-Lorenzo, M.; Wang, Z.; Kong, X.-T.; Govorov, A. O.; Correa-Duarte, M. A. Boosting hot electron-driven photocatalysis through anisotropic plasmonic nanoparticles with hot spots in Au−TiO2 nanoarchitectures. *J. Phys. Chem. C* **2016**, *120*, 11690.
(50) Punj, D.; de Torres, J.; Rigneault, H.; Wenger, J. Gold nanoparticles for enhanced single molecule fluorescence analysis at micromolar concentration. *Opt. Express* **2013**, *21*, 27338.
(51) Swaim, J. D.; Knittel, J.; Bowen, W. P. Detection limits in whispering gallery biosensors with plasmonic enhancement. *Appl. Phys. Lett.* **2011**, *99*, 243109.
(52) Mori, T.; Yamaguchi, K.; Tanaka, Y.; Suzaki, Y.; Haraguchi, M. Optical characteristics of rounded silver nanoprisms. *Optical Review* **2016**, *23*, 260.
(53) Salmón-Gamboa, J. U.; Romero-Gómez, M.; Roth, D. J.; Krasavin, A. V.; Wang, P.; Dickson, W.; Zayats, A. V. Rational design of bimetallic photocatalysts based on plasmonically-derived hot carriers. *Nanoscale Advances* **2021**, *3*, 767.
(54) Córdova-Castro, R. M.; Krasavin, A. V.; Nasir, M. E.; Zayats, A. V.; Dickson, W. Nanocone-based plasmonic metamaterials. *Nanotechnology* **2019**, *30*, 055301.
(55) Kinkhabwala, A.; Yu, Z.; Fan, S.; Avlasevich, Y.; Müllen, K.; Moerner, W. Large single-molecule fluorescence enhancements produced by a bowtie nanoantenna. *Nat. Photonics* **2009**, *3*, 654.
(56) Khan, A. U.; Zhao, S.; Liu, G. Key parameter controlling the sensitivity of plasmonic metal nanoparticles: aspect ratio. *J. Phys. Chem. C* **2016**, *120*, 19353.
(57) Richtmyer, R. Dielectric resonators. *J. Appl. Phys.* **1939**, *10*, 391.
(58) Foreman, M. R.; Swaim, J. D.; Vollmer, F. Whispering gallery mode sensors. *Adv. Opt. Photon.* **2015**, *7*, 168.
(59) Gu, F.; Xie, F.; Lin, X.; Linghu, S.; Fang, W.; Zeng, H.; Tong, L.; Zhuang, S. Single whispering-gallery mode lasing in polymer bottle microresonators via spatial pump engineering. *Light Sci. Appl.* **2017**, *6*, No. e17061.
(60) Druger, S. D.; Arnold, S.; Folan, L. M. Theory of enhanced energy transfer between molecules embedded in spherical dielectric particles. *J. Chem. Phys.* **1987**, *87*, 2649.
(61) Shopova, S.; Blackledge, C.; Rosenberger, A. Enhanced evanescent coupling to whispering-gallery modes due to gold nanorods grown on the microresonator surface. *Appl. Phys. B: Laser Opt.* **2008**, *93*, 183.
(62) Kaplan, A.; Tomes, M.; Carmon, T.; Kozlov, M.; Cohen, O.; Bartal, G.; Schwefel, H. G. Finite element simulation of a perturbed axial-symmetric whispering-gallery mode and its use for intensity enhancement with a nanoparticle coupled to a microtoroid. *Opt. Express* **2013**, *21*, 14169.
(63) Bozzola, A.; Perotto, S.; De Angelis, F. Hybrid plasmonic−photonic whispering gallery mode resonators for sensing: a critical review. *Analyst* **2017**, *142*, 883.
(64) Zhu, J.; Ozdemir, S. K.; Xiao, Y.-F.; Li, L.; He, L.; Chen, D.-R.; Yang, L. On-chip single nanoparticle detection and sizing by mode splitting in an ultrahigh-Q microresonator. *Nat. Photonics* **2010**, *4*, 46.
(65) Vollmer, F.; Arnold, S.; Keng, D. Single virus detection from the reactive shift of a whispering-gallery mode. *Proc. Natl. Acad. Sci. U.S.A.* **2008**, *105*, 20701.
(66) Santiago-Cordoba, M. A.; Cetinkaya, M.; Boriskina, S. V.; Vollmer, F.; Demirel, M. C. Ultrasensitive detection of a protein by optical trapping in a photonic-plasmonic microcavity. *J. Biophotonics* **2012**, *5*, 629.
(67) Shopova, S.; Rajmangal, R.; Nishida, Y.; Arnold, S. Ultrasensitive nanoparticle detection using a portable whispering gallery mode biosensor driven by a periodically poled lithium-niobate frequency doubled distributed feedback laser. *Rev. Sci. Instrum.* **2010**, *81*, 103110.
(68) Lu, T.; Lee, H.; Chen, T.; Herchak, S.; Kim, J.-H.; Fraser, S. E.; Flagan, R. C.; Vahala, K. High sensitivity nanoparticle detection using optical microcavities. *Proc. Natl. Acad. Sci. U.S.A.* **2011**, *108*, 5976.
(69) Su, J. Label-free single exosome detection using frequency-locked microtoroid optical resonators. *ACS Photonics* **2015**, *2*, 1241.
(70) Su, J.; Goldberg, A. F.; Stoltz, B. M. Label-free detection of single nanoparticles and biological molecules using microtoroid optical resonators. *Light Sci. Appl.* **2016**, *5*, No. e16001.
(71) Nadgaran, H.; Afkhami Garaei, M. Enhancement of a whispering gallery mode microtoroid resonator by plasmonic triangular gold nanoprism for label-free biosensor applications. *J. Appl. Phys.* **2015**, *118*, 043101.
(72) Arnold, S.; Dantham, V. R.; Barbre, C.; Garetz, B. A.; Fan, X. Periodic plasmonic enhancing epitopes on a whispering gallery mode biosensor. *Opt. Express* **2012**, *20*, 26147.
(73) Dantham, V. R.; Holler, S.; Barbre, C.; Keng, D.; Kolchenko, V.; Arnold, S. Label-free detection of single protein using a nanoplasmonic-photonic hybrid microcavity. *Nano Lett.* **2013**, *13*, 3347.
(74) Ahmed, R.; Rifat, A. A.; Yetisen, A. K.; Salem, M. S.; Yun, S.-H.; Butt, H. Optical microring resonator based corrosion sensing. *RSC Adv.* **2016**, *6*, 56127.
(75) Urbonas, D.; Balčytis, A.; Gabalis, M.; Vaškevičius, K.; Naujokaite, G.; Juodkazis, S.; Petruškevičius, R. Ultra-wide free spectral range, enhanced sensitivity, removed mode splitting SOI optical ring resonator with dispersive metal nanodisks. *Opt. Lett.* **2015**, *40*, 2977.
(76) Baaske, M. D.; Vollmer, F. Optical observation of single atomic ions interacting with plasmonic nanorods in aqueous solution. *Nat. Photonics* **2016**, *10*, 733.
(77) Vincent, S.; Subramanian, S.; Vollmer, F. Optoplasmonic characterisation of reversible disulfide interactions at single thiol sites in the attomolar regime. *Nat. Commun.* **2020**, *11*, 1.
(78) Zhou, N.; Wang, P.; Shi, Z.; Gao, Y.; Yang, Y.; Wang, Y.; Xie, Y.; Cai, D.; Guo, X.; Zhang, L.; et al. Au nanorod−coupled microfiber optical humidity sensors. *Opt. Express* **2019**, *27*, 8180.
(79) Deng, H.; Haug, H.; Yamamoto, Y. Exciton-polariton bose-einstein condensation. *Reviews of modern physics* **2010**, *82*, 1489.
(80) Liu, X.; Galfsky, T.; Sun, Z.; Xia, F.; Lin, E.-c.; Lee, Y.-H.; Kéna-Cohen, S.; Menon, V. M. Strong light−matter coupling in two-dimensional atomic crystals. *Nat. Photonics* **2015**, *9*, 30.
(81) Törmä, P.; Barnes, W. L. Strong coupling between surface plasmon polaritons and emitters: a review. *Rep. Prog. Phys.* **2015**, *78*, 013901.
(82) Novotny, L. Strong coupling, energy splitting, level crossings: A classical perspective. *American Journal of Physics* **2010**, *78*, 1199.
(83) Baranov, D. G.; Wersall, M.; Cuadra, J.; Antosiewicz, T. J.; Shegai, T. Novel nanostructures and materials for strong light−matter interactions. *ACS Photon.* **2018**, *5*, 24.
(84) Jin, Y.; Yang, L.; Pan, C.; Shi, Z.; Cui, B.; Xu, P.; Yang, Y.; Zhou, N.; Guo, X.; Wang, P.; Tong, L. Strong coupling of a plasmonic nanoparticle to a semiconductor nanowire. *Nanophotonics* **2021**, *10*, 2875.
(85) Faucheaux, J. A.; Fu, J.; Jain, P. K. Unified theoretical framework for realizing diverse regimes of strong coupling between plasmons and electronic transitions. *J. Phys. Chem. C* **2014**, *118*, 2710.
(86) Martinsson, E.; Sepulveda, B.; Chen, P.; Elfwing, A.; Liedberg, B.; Aili, D. Optimizing the refractive index sensitivity of plasmonically coupled gold nanoparticles. *Plasmonics* **2014**, *9*, 773.
(87) Farooq, S.; Rativa, D.; de Araujo, R. E. High performance gold dimeric nanorods for plasmonic molecular sensing. *IEEE Sensors Journal* **2021**, *21*, 13184.
(88) Iqbal, M.; Gleeson, M. A.; Spaugh, B.; Tybor, F.; Gunn, W. G.; Hochberg, M.; Baehr-Jones, T.; Bailey, R. C.; Gunn, L. C. Label-free biosensor arrays based on silicon ring resonators and high-speed optical scanning instrumentation. *IEEE J. Sel. Top. Quantum Electron.* **2010**, *16*, 654.

(89) Lee, H.; Chen, T.; Li, J.; Yang, K. Y.; Jeon, S.; Painter, O.; Vahala, K. J. Chemically etched ultrahigh-Q wedge-resonator on a silicon chip. *Nat. Photonics* **2012**, *6*, 369.
(90) Benson, O. Assembly of hybrid photonic architectures from nanophotonic constituents. *Nature* **2011**, *480*, 193.
(91) Yang, L.; Wang, H.; Fang, Y.; Li, Z. Polarization state of light scattered from quantum plasmonic dimer antennas. *ACS Nano* **2016**, *10*, 1580.
(92) Muskens, O. L.; Giannini, V.; Sánchez-Gil, J.; Rivas, J. G. Optical scattering resonances of single and coupled dimer plasmonic nanoantennas. *Opt. Express* **2007**, *15*, 17736.
(93) Lu, G.; Wang, Y.; Chou, R. Y.; Shen, H.; He, Y.; Cheng, Y.; Gong, Q. Directional side scattering of light by a single plasmonic trimer. *Laser Photon. Rev.* **2015**, *9*, 530.
(94) Chuntonov, L.; Haran, G. Trimeric plasmonic molecules: the role of symmetry. *Nano Lett.* **2011**, *11*, 2440.
(95) Arbabi, E.; Kamali, S. M.; Arnold, S.; Goddard, L. L. Hybrid whispering gallery mode/plasmonic chain ring resonators for biosensing. *Appl. Phys. Lett.* **2014**, *105*, 231107.
(96) Scofield, A. C.; Kim, S.-H.; Shapiro, J. N.; Lin, A.; Liang, B.; Scherer, A.; Huffaker, D. L. Bottom-up photonic crystal lasers. *Nano Lett.* **2011**, *11*, 5387.
(97) Minamisawa, R. A.; Süess, M. J.; Spolenak, R.; Faist, J.; David, C.; Gobrecht, J.; Bourdelle, K. K.; Sigg, H. Top-down fabricated silicon nanowires under tensile elastic strain up to 4.5%. *Nat. Commun.* **2012**, *3*, 1.
(98) Li, G.-C.; Lei, D.; Qiu, M.; Jin, W.; Lan, S.; Zayats, A. V. Light-induced symmetry breaking for enhancing second-harmonic generation from an ultrathin plasmonic nanocavity. *Nat. Commun.* **2021**, *12*, 1.
(99) Cardano, F.; Marrucci, L. ″Spin−orbit photonics,″. *Nat. Photonics* **2015**, *9*, 776.
(100) O'connor, D.; Ginzburg, P.; Rodríguez-Fortuño, F. J.; Wurtz, G. A.; Zayats, A. V. Spin−orbit coupling in surface plasmon scattering by nanostructures. *Nat. Commun.* **2014**, *5*, 1.
(101) Chen, P.; Lo, T. W.; Fan, Y.; Wang, S.; Huang, H.; Lei, D. Chiral coupling of valley excitons and light through photonic spin−orbit interactions. *Adv. Opt. Mater.* **2020**, *8*, 1901233.
(102) Lodahl, P.; Mahmoodian, S.; Stobbe, S.; Rauschenbeutel, A.; Schneeweiss, P.; Volz, J.; Pichler, H.; Zoller, P. Chiral quantum optics. *Nature* **2017**, *541*, 473.
(103) Lin, W.; Ota, Y.; Iwamoto, S.; Arakawa, Y. Spin-dependent directional emission from a quantum dot ensemble embedded in an asymmetric waveguide. *Opt. Lett.* **2019**, *44*, 3749.
(104) Chen, P.-G.; Li, Z.; Qi, Y.; Lo, T. W.; Wang, S.; Jin, W.; Wong, K.-Y.; Fan, S.; Zayats, A. V.; Lei, D. Long-Range Directional Routing and Spatial Selection of High-Spin-Purity Valley Trion Emission in Monolayer WS2. *ACS Nano* **2021**, *15*, 18163.
(105) Yang, X.-C.; Yu, H.; Yao, W. Chiral Excitonics in Monolayer Semiconductors on Patterned Dielectrics. *Phys. Rev. Lett.* **2022**, *128*, 217402.
(106) Chen, W.; Kaya Özdemir, Ş.; Zhao, G.; Wiersig, J.; Yang, L. Exceptional points enhance sensing in an optical microcavity. *Nature* **2017**, *548*, 192.
(107) Zhong, Q.; Kou, J.; Özdemir, Ş.; El-Ganainy, R. Hierarchical construction of higher-order exceptional points. *Phys. Rev. Lett.* **2020**, *125*, 203602.
(108) Langbein, W. No exceptional precision of exceptional-point sensors. *Phys. Rev. A* **2018**, *98*, 023805.
(109) Zhang, M.; Sweeney, W.; Hsu, C. W.; Yang, L.; Stone, A.; Jiang, L. Quantum noise theory of exceptional point amplifying sensors. *Phys. Rev. Lett.* **2019**, *123*, 180501.
(110) Peng, B.; Özdemir, Ş. K.; Liertzer, M.; Chen, W.; Kramer, J.; Yılmaz, H.; Wiersig, J.; Rotter, S.; Yang, L. Chiral modes and directional lasing at exceptional points. *Proc. Natl. Acad. Sci. U.S.A.* **2016**, *113*, 6845.
(111) Zhang, P.-J.; Ji, Q.-X.; Cao, Q.-T.; Wang, H.; Liu, W.; Gong, Q.; Xiao, Y.-F. Single-mode characteristic of a supermode microcavity Raman laser. *Proc. Natl. Acad. Sci. U.S.A.* **2021**, *118*, e2101605118.

https://doi.org/10.1021/acsphotonics.2c01271
ACS Photonics 2023, 10, 2−12